JGR Planets

RESEARCH ARTICLE
10.1029/2025JE009479

Cooling History of Chang'e-5 Basalts Recorded by Diffusion-Driven Mg and Fe Isotope Fractionation

K. Shuai[1,2], J. Chen[3], S. Boschi[3], H. Hui[3,4,5], and W. Li[3,4]

[1]School of Astronomy and Space Science, Nanjing University, Nanjing, China, [2]Key Laboratory of Modern Astronomy and Astrophysics in Ministry of Education, Nanjing University, Nanjing, China, [3]State Key Laboratory of Critical Earth Material Cycling and Mineral Deposits, School of Earth Sciences and Engineering, Nanjing University, Nanjing, China, [4]CAS Center for Excellence in Comparative Planetology, Hefei, China, [5]CAS Key Laboratory of Earth and Planetary Physics, Institute of Geology and Geophysics, Chinese Academy of Sciences, Beijing, China

Abstract The basalt clasts returned by the Chang'e-5 (CE-5) mission recorded a spatial diversity of cooling histories, with various cooling rates and timescales reported for different clasts. However, the temporal evolution of thermal conditions during cooling has received limited attention. Here, we report ∼0.3‰ and ∼0.8‰ in δ^{56}Fe and δ^{26}Mg variability at the mineral-grain scale in a CE-5 basalt clast, which are negatively correlated, unambiguously pinpointing kinetic isotope fractionation driven by inter-diffusion in the minerals. Combined with systematic diffusion modeling and grain size analysis, the Mg–Fe isotopic variability reveals a substantial decrease in the cooling rate from 30–100°C/day to 1–10°C/day during the crystallization and cooling of the clast. The change in thermal conditions during eruption or magma overlaying caused the cooling rate to decrease. Our results highlight the importance of temporal evolution of thermal conditions in the crystallization and cooling history of magmatic systems.

Plain Language Summary Basalt fragments (clasts) returned by the Chang'e-5 mission to the Moon preserve records of their crystallization and cooling history. Previous studies showed that different clasts cooled at varying rates, indicating diverse thermal environments within the magmatic system. In this study, we examine how thermal conditions changed over time for a single basalt clast. The isotopic signatures in different mineral grains in this clast reflect diffusion of iron and magnesium ions under different thermal conditions. Minerals that formed early cooled rapidly, while those that formed later cooled more slowly. This slowdown in cooling rate reveals a complex path of thermal evolution for the clast.

Key Points:

- Remarkable and negatively correlated δ^{26}Mg and δ^{56}Fe variability at the mineral scale is observed in a Chang'e-5 basalt clast
- Chemical diffusion in mineral grains within a cooling melt caused the isotopic variability
- The cooling rate decreased over time, which reveals the temporal evolution of thermal conditions

Supporting Information:

Supporting Information may be found in the online version of this article.

Correspondence to:

W. Li,
liweiqiang@nju.edu.cn

Citation:

Shuai, K., Chen, J., Boschi, S., Hui, H., & Li, W. (2026). Cooling history of Chang'e-5 basalts recorded by diffusion-driven Mg and Fe isotope fractionation. *Journal of Geophysical Research: Planets*, *131*, e2025JE009479. https://doi.org/10.1029/2025JE009479

Received 5 OCT 2025
Accepted 21 APR 2026

Author Contributions:

Conceptualization: W. Li
Formal analysis: K. Shuai
Funding acquisition: W. Li
Investigation: K. Shuai, J. Chen, S. Boschi, W. Li
Methodology: K. Shuai, J. Chen, S. Boschi
Resources: W. Li
Software: K. Shuai
Supervision: W. Li
Visualization: K. Shuai
Writing – original draft: K. Shuai
Writing – review & editing: K. Shuai, S. Boschi, H. Hui, W. Li

1. Introduction

Lunar volcanism, one of the major processes occurring on the Moon after the magma ocean solidification, reflects the thermal-chemical evolution of the Moon (Shearer, 2006). The basalt clasts returned by the Chang'e-5 (CE-5) mission represent the youngest lunar basalts so far, with ages of ∼2.0 Ga (Boschi et al., 2023; Che et al., 2021; Q.-L. Li et al., 2021), providing key insights into the evolution of volcanic activity on the Moon. The magmatic evolution history of CE-5 basalts has been investigated from the perspectives of mineral abundance, texture, chemical composition, and radioisotopes. Their parental melts are likely to be highly evolved with extensive fractional crystallization after low-degree melting of the mantle source (Tian et al., 2021). In addition, clinopyroxene thermobarometry and magmatic evolution modeling suggest that the parental melt of CE-5 basalts was generated at ∼250 km depth and 1350°C (Luo et al., 2023). Most pyroxene and olivine grains in CE-5 basalts show compositional zoning (Tian et al., 2021), which has been used to estimate the rate and timescale of magma cooling (Luo et al., 2023; Tian et al., 2023; Z. Wang, Wang, et al., 2023).

Iron and magnesium isotope signatures have proven effective in tracing the lunar magma ocean differentiation (Liu et al., 2010; Poitrasson et al., 2019; Sedaghatpour & Jacobsen, 2019; Sedaghatpour et al., 2013; Sossi & Moynier, 2017; K. Wang et al., 2015; Weyer et al., 2005) and space weathering processes on the Moon (Okabayashi et al., 2019; Wiesli et al., 2003). For CE-5 basalts, its Mg isotopic composition lies within the range of low-Ti mare basalts and Fe isotopic composition between low-Ti and high-Ti mare basalts, indicating a hybrid mantle source (Jiang et al., 2023). In situ analysis of Fe isotopes in CE-5 basalt clasts shows light Fe isotopic composition of olivines relative to ilmenites and isotopically light rims in olivines, implying chemical diffusion at the mineral scale (Y. Li et al., 2025). However, a quantitative understanding of the connection between the magmatic processes and the isotopic fractionation in CE-5 basalts is still lacking.

Studies based on terrestrial samples demonstrate that Fe–Mg inter-diffusion between minerals and melt can result in unique Fe and Mg isotopic signatures that can be exploited to quantify the cooling history of magmas (Dauphas et al., 2010; Oeser et al., 2015; Sio & Dauphas, 2017; Sio et al., 2013; Teng et al., 2011; Tian et al., 2020). Particularly, the time-temperature cooling paths of magmatic bodies can be quantitatively constrained using the diffusion-driven isotopic fractionation (Sio & Dauphas, 2017). For CE-5 basalts, diverse cooling histories of different clasts have been revealed (Jiang et al., 2022; Jin et al., 2024; Luo et al., 2023; Neal et al., 2022; Tian et al., 2023; Z. Wang, Tian, et al., 2023; Z. Wang, Wang, et al., 2023; Webb et al., 2022), reflecting a spatial variation of the thermal conditions in the magmatic system. However, a single cooling rate or timescale was reported for each clast, thus not capturing the temporal evolution of thermal conditions.

To investigate the cooling history and the thermal condition evolution of CE-5 basalts, we measured the Fe and Mg isotopic compositions in mineral separates of a CE-5 basalt clast. Systematic diffusion modeling was conducted to determine the key parameters that control the diffusion-induced isotope fractionation and quantitatively constrain the cooling path of the studied clast.

2. Methods

2.1. Sample and Methods of Grain Size Measurements

We studied a CE-5 granular basalt clast (#CE5C0000YJYX048) with ∼3 mm in size, 17.6 mg in weight, and poikilitic texture. The minerology, Pb-Pb age, and K isotopic composition of this clast have been reported by Boschi et al. (2023) and An et al. (2023). The details of sample preparation for isotope analysis are described in An et al. (2023). The tomographic slice images of the clast obtained with high-resolution X-ray tomographic microscopy (HR-XRTM) by Boschi et al. (2023) were used for 3D measurement of olivine grain sizes. There are 3,001 projections (tomographic slices) in total, with a voxel (pixel) size of 1.7 μm. Minerals are characterized by different gray values in these images. Other details of HR-XRTM were reported by Boschi et al. (2023). We manually identified the outlines of the olivine grains larger than 20 μm in each slice, reconstructing the 3D surfaces of these grains (Movie S1). The outlines of these grains were processed using the BoneJ plugin in the ImageJ software (Doube, 2021). The volume of each grain was measured precisely. Each olivine grain was fitted with an ellipsoid. The intermediate radius of the best-fit ellipsoid was used to represent the radius of the grain.

2.2. Iron and Magnesium Isotope Analysis

The clast was gently crushed between two glass slides. Different phases were separated using tweezers under a binocular microscope for subsequent chemical and isotopic analyses. Mineral separates of olivine, ilmenite, plagioclase, and pyroxene were collected for Fe and Mg isotope analysis, with each aliquot of mineral sample consisting of mineral grains that weighed 100–300 μg. We did not perform any additional processing or characterization of the mineral separates to avoid environmental contamination. Although care was taken during mineral picking, the complete separation of tiny mineral grains is difficult due to mineral intergrowth. We calculated the mineral abundance in each mineral separate based on the compositions of minerals in the studied clast (Boschi et al., 2023). The effects of mixing with minor other minerals in each mineral separate on our results are discussed in Supporting Information S1.

The Fe and Mg isotopic compositions of the mineral separates were measured at the State Key Laboratory for Critical Earth Material Cycling and Mineral Deposits, Nanjing University. Details of the procedures for column chemistry and isotope measurement are described in Brzozowski et al. (2022) and Du et al. (2024) for Mg and Fe, respectively. Briefly, the mineral separates were digested in Teflon beakers using 1:1 mixture of concentrated HNO_3–HF. The sample solutions were dried and re-dissolved in 7 M HCl. An aliquot of each sample solution was taken and measured for major element concentrations on an inductively coupled plasma optical emission spectrometer (ICP-OES). The chloride-form AG MP-1 anion-exchange resin (100–200 mesh, 0.2 mL) was used for Fe purification. Magnesium was purified from the matrix fraction obtained from Fe purification, using the AG 50W-X100 resin (100–200 mesh, 1 mL) and the AG 50W-X8 resin (100–200 mesh, 0.2 mL). The Fe and Mg isotope measurements were conducted on a Nu 1700 Sapphire multi-collector inductively coupled plasma mass spectrometer (MC-ICP-MS). Standard sample bracketing was used to correct for instrumental mass bias. Iron isotopes (^{54}Fe, ^{56}Fe, and ^{57}Fe) were measured at medium resolution (m/Δm of ∼8,000). The isobaric interference of $^{54}Cr^{+}$ on $^{54}Fe^{+}$ was monitored by measuring $^{50}Cr^{+}$ and an online correction was applied. Iron isotopic compositions are reported relative to IRMM-014:

$$\delta^{56}\mathrm{Fe}_{\mathrm{sample}}(‰) = \left[\left({}^{56}\mathrm{Fe}/{}^{54}\mathrm{Fe}\right)_{\mathrm{sample}}/\left({}^{56}\mathrm{Fe}/{}^{54}\mathrm{Fe}\right)_{\mathrm{IRMM-014}}\right] \times 1000. \quad (1)$$

Magnesium isotopes (^{24}Mg, ^{25}Mg, and ^{26}Mg) were measured at low resolution, with the Mg isotopic compositions reported relative to DSM-3:

$$\delta^{26}\mathrm{Mg}_{\mathrm{sample}}(‰) = \left[\left({}^{26}\mathrm{Mg}/{}^{24}\mathrm{Mg}\right)_{\mathrm{sample}}/\left({}^{26}\mathrm{Mg}/{}^{24}\mathrm{Mg}\right)_{\mathrm{DSM-3}}\right] \times 1000. \quad (2)$$

The Mg and Fe isotope composition of geologic standards (Table S1 in Supporting Information S1), which were purified and analyzed as unknowns together with the samples, are in excellent agreement with the reference values (e.g., He et al., 2015; Teng et al., 2015).

2.3. Magmatic Evolution Modeling

To obtain the relation between temperature and composition of mineral grains during diffusion, we modeled the magmatic evolution of CE-5 basalts using the MELTS software (Asimow & Ghiorso, 1998; Ghiorso & Sack, 1995). The bulk composition of the studied clast is unlikely to represent the composition of its parental melts (Boschi et al., 2023); thus, it is not suitable to be used as the initial composition of magmatic evolution. We used the bulk composition of a CE-5 basalt clast (042GP-002 in Tian et al., 2021) with high Mg# (100 × molar Mg/(Mg + Fe)) as the initial composition. The oxygen fugacity of IW–0.84 (H. Zhang et al., 2024) was used for modeling. The pressure is assumed to be linearly correlated with temperature before the pressure decreases to zero. This correlation was estimated using the reported pressure and temperature of CE-5 clinopyroxenes (Luo et al., 2023). The magmatic evolution modeling yielded the crystallization temperature of phases with different compositions, which were used in diffusion modeling.

2.4. Modeling Isotope Fractionation Driven by Fe-Mg Inter-Diffusion

The Fe-Mg inter-diffusion and the diffusion-driven isotope fractionation were modeled following Dauphas et al. (2010) and Sio et al. (2013). The partial differential equation of the spherical diffusion process is:

$$\frac{\partial C(t,r)}{\partial t} = \frac{1}{r^2}\frac{\partial}{\partial r}\left[r^2 D \frac{\partial C(t,r)}{\partial r}\right], \quad (3)$$

where t is time, r is the distance to the center of a grain, D is diffusion coefficient, and C is concentration, which is the function of r and t. This governing equation was solved numerically using a finite-difference scheme. The diffusion coefficients of two isotopes (D_1 and D_2) with masses of m_1 and m_2 are related by $D_1/D_2 = (m_2/m_1)^{\beta}$, where β is an empirical constant (Richter et al., 2009). The β value plays a key role in controlling the magnitude of diffusion-driven isotope fractionation, with higher β values leading to more pronounced isotope fractionation (Sio et al., 2013; Xiong et al., 2023). The β values of 0.16 for Fe and 0.09 for Mg (Oeser et al., 2015; Sio et al., 2018) were used in our nominal model. Other β values (Oeser et al., 2026; Sio et al., 2013) were tested to assess the effects of varying β values and potential anisotropy (Supporting Information S1).

The boundary conditions include the initial concentration C_0, surface concentration C_1, and the zero flux at the center of the grain:

$$\begin{cases} C(0,r) = C_0 \\ C(t,a) = C_1 \\ \left[\dfrac{\partial C(t,r)}{\partial r}\right]_{r=0} = 0 \end{cases}, \quad (4)$$

where a is the grain radius. Using the concentrations of the isotopes in each incremental distance, the isotopic compositions (δ) can be derived. The bulk grain isotope compositions (δ_{bulk}) were calculated as follows:

$$\delta_{\text{bulk}} = \frac{\int_0^a \delta(r)\, C(r)\, r^2 \mathrm{d}r}{\int_0^a C(r)\, r^2 \mathrm{d}r}. \quad (5)$$

We modeled the isotope fractionation driven by Fe-Mg inter-diffusion in olivine grains to reproduce the measured isotopic data. Varying grain sizes, cooling rates, and initial Mg# of olivine were used in different sets of simulations. The initial Mg# is defined as the Mg# of olivine at the onset of diffusion, representing the composition established during crystallization. The diffusion coefficient was calculated based on the given temperature, pressure, and oxygen fugacity (IW–0.84; H. Zhang et al., 2024), and the Mg# value (Dohmen & Chakraborty, 2007). At each time and space step, the same Mg# value was used in the diffusion coefficient calculation for all isotopes. The grain radii in diffusion modeling vary from 20 to 1,000 μm, covering the dominant radii of olivine grains in the clast. A linear cooling model was used in the diffusion model (Dauphas et al., 2010). Different cooling rates from 1 to 1000°C/day were used.

The relationship between Mg# and temperature modeled using MELTS was used to constrain the initial and boundary conditions in the diffusion model. The temperatures of olivine crystallization with different Mg# were used as the initial temperatures of diffusion, and the temperature at the end of crystallization (1024°C) was set as the final temperature. The surface Mg# was assumed to be the same as the Mg# of olivine crystallizing at different temperatures. The final surface Mg# is 3.8, similar to the lowest Mg# of olivine samples (2.4). The detailed boundary conditions and procedure of diffusion modeling are presented in Supporting Information S1.

3. Results

The 3D reconstruction and measurement (Movie S1) show that the olivine grains with radii of 100–300 μm make up the majority of the volume of olivines in the clast. Based on the major element data, the bulk Mg# of each sample was calculated (Table S2 in Supporting Information S1). Most samples have Mg# lower than 25, except for two olivine samples (F112 and F122) with high Mg# of 44.9 and 41.8. Due to mineral intergrowth, complete separation of individual mineral grains from the tiny clast is challenging, and contamination by other phases is unavoidable. Most of our mineral separates are mixtures of multiple phases (Table S3 in Supporting Information S1). Importantly, the three olivine-rich separates for quantitative comparison with modeling results (F112, F122, and F123) have high olivine abundances and low pyroxene and ilmenite abundances. Their Mg#, δ^{56}Fe, and δ^{26}Mg values are not substantially affected by minor contamination and thus reflect their crystallization and thermal histories.

Both δ^{26}Mg and δ^{56}Fe of the mineral separates are highly variable (Table S1 in Supporting Information S1; Figure 1), with values both above and below the bulk isotopic compositions of CE-5 basalts (δ^{56}Fe = 0.107 ± 0.007‰ and δ^{26}Mg = −0.264 ± 0.015‰) (Jiang et al., 2023). The pyroxene, plagioclase, and ilmenite samples have similar δ^{56}Fe of 0.14–0.25‰, whereas the olivine samples show greater variation in δ^{56}Fe (−0.05–0.17‰). The two olivine samples with high Mg# show δ^{56}Fe of 0.05 ± 0.04‰ and −0.05 ± 0.02‰, lower than those of all other samples. The δ^{56}Fe of ilmenite samples are higher than those of olivine, consistent with the published in situ data (Y. Li et al., 2025). The pyroxene samples had the lowest δ^{26}Mg in all measured samples, varying from −0.53 to −0.18‰. Two ilmenite samples show similar δ^{26}Mg of ∼0.05‰ and the olivine samples show varying δ^{26}Mg from −0.14 to 0.31‰. Particularly, there is a negative correlation between δ^{56}Fe and δ^{26}Mg for the mineral separates, which yields a coefficient of determination (R^2) of 0.34 from a simple linear regression, and δ^{56}Fe is negatively correlated with Mg# with R^2 of 0.52 (Figure 1). Note that simple linear regressions do not account for the Mg#-dependence of the correlations, as discussed in Section 4.2.

The magmatic evolution modeling yielded the crystallization temperatures of olivines with different chemical compositions (Figure S1 in Supporting Information S1). Olivine crystallization starts at 1134°C with Mg# of 50.3 and continues until the temperature reaches 1024°C with an almost pure fayalitic composition (Mg# of 3.8). The modeled low Mg content in olivines and low olivine abundance (∼8 wt%) are consistent with literature data for CE-5 samples (Boschi et al., 2023; C. Li et al., 2022; Qian et al., 2023; Tian et al., 2021).

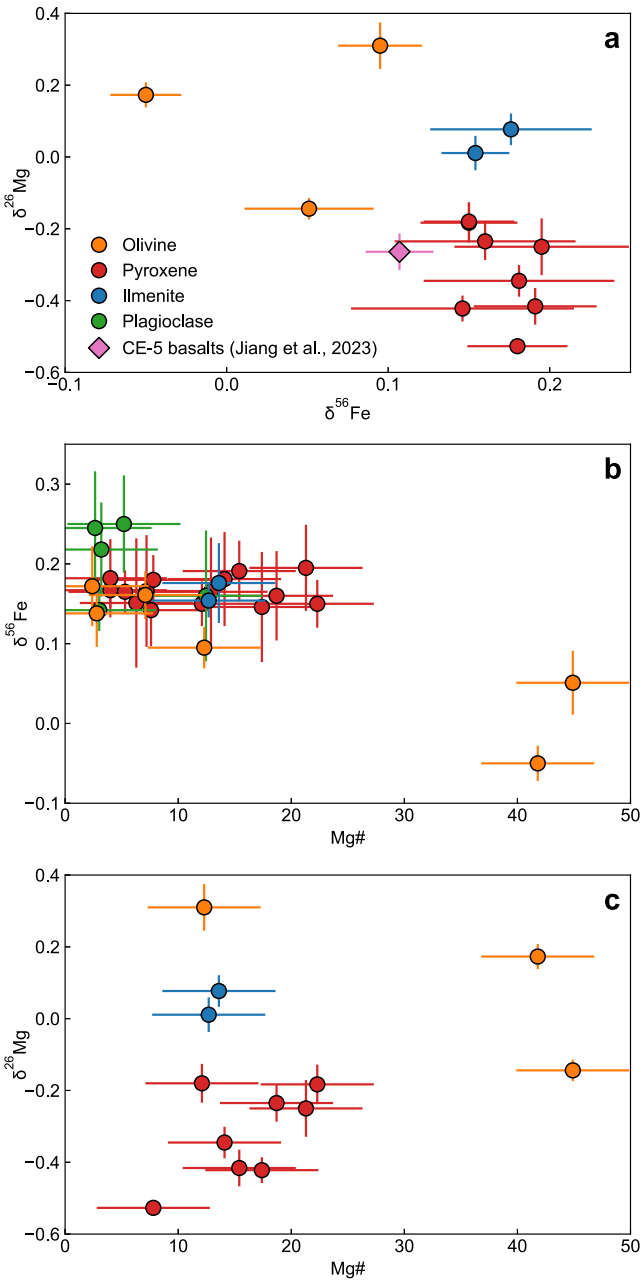

Figure 1. Isotopic compositions and Mg# of the mineral separated. (a) δ^{26}Mg versus δ^{56}Fe of the mineral separates. Published isotopic compositions of bulk CE-5 basalts (Jiang et al., 2023) are plotted for comparison. (b) δ^{56}Fe versus Mg#. (c) δ^{26}Mg versus Mg#.

4. Discussion

4.1. Chemical Diffusion-Driven Fe and Mg Isotope Fractionation

The Fe and Mg isotopic compositions of the mineral separates from one single basaltic clast are highly variable, with variability of ~0.3‰ and ~0.8‰ for δ^{56}Fe and δ^{26}Mg, respectively. The highest δ^{26}Mg (0.31 ± 0.07‰) exceeds the highest δ^{26}Mg of bulk lunar rocks (0.082 ± 0.021‰; Sedaghatpour & Jacobsen, 2019). The lowest δ^{56}Fe (−0.05 ± 0.02‰) is lower than the δ^{56}Fe of most lunar rock samples, except for a dunite sample (72415), which was affected by diffusion-induced isotope fractionation in olivine (K. Wang et al., 2015). Therefore, mixing of melts from different sources cannot produce the observed isotopic variations.

Equilibrium isotope fractionation, Soret diffusion, and chemical diffusion are the possible processes that can result in the Fe and Mg isotopic variations at high temperatures (Dauphas et al., 2010; Huang et al., 2010; Richter et al., 2009; Shahar et al., 2008). Under isotope equilibrium, inter-mineral Fe and Mg isotope fractionation is small (Teng et al., 2007). The inter-mineral equilibrium isotope fractionation at high temperature can be calculated using the reduced partition function ratios (W. Wang, Wu, et al., 2023). At the temperature of the parental melts of CE-5 basalts (>1024°C), the equilibrium Mg isotope fractionation between olivine and clinopyroxene is <0.12‰. The equilibrium Fe isotope fractionation between olivine and melts is ~0.03‰ at 1130°C (Dauphas et al., 2014). Therefore, equilibrium isotope fractionation cannot be the cause of the observed isotopic variations. Soret diffusion can also be ruled out because this process will lead to a positive correlation between δ^{56}Fe and δ^{26}Mg (Huang et al., 2010; Richter et al., 2009), which is inconsistent with the observed negative isotopic correlation (Figure 1).

Chemical inter-diffusion of Fe and Mg, on the contrary, could result in the observed isotopic variations. During differentiation of a magma, iron tends to diffuse from the evolving melt into mafic silicate minerals (e.g., olivine) and iron oxides, while Mg diffuses out of the minerals (Dauphas et al., 2010; Oeser et al., 2015; Sio et al., 2013; Teng et al., 2011; Tian et al., 2020), leading to kinetic isotope fractionation in the mineral grains. For CE-5 basalt, this inter-diffusion is evidenced by the compositional zoning observed in olivines and clinopyroxenes, with the mineral core showing higher Mg# than the rim (Luo et al., 2023; Tian et al., 2021, 2023). The isotope fractionation is driven by mass-dependent differences in the diffusion coefficients of the isotopes; thus, the diffusion of Fe and Mg in opposite directions leads to a negative correlation between δ^{56}Fe and δ^{26}Mg in the minerals (Dauphas et al., 2010; Richter et al., 2009; Teng et al., 2011; Tian et al., 2020). Our results show a negative correlation between δ^{56}Fe and δ^{26}Mg, demonstrating that the observed isotopic variation resulted from Fe–Mg inter-diffusion.

The variable Mg# and isotopic compositions in the studied clast reflect different diffusion processes. The two olivine samples with high Mg# (F112 and F122) may be composed of early-formed olivines. They have Mg# values of 41.8 and 44.9 with negative δ^{56}Fe fractionation and positive δ^{26}Mg fractionation relative to bulk CE-5 basalts. For olivines with an Mg# of ~50, Fe–Mg inter-diffusion is expected to produce Fe and Mg isotope fractionation of comparable magnitude but opposite directions (Dauphas et al., 2010), consistent with the measured data of F112 and F122.

All other samples are low in Mg#, including pyroxenes (mainly Fe-rich pigeonites), plagioclase, ilmenite, and low-Mg# olivines (fayalite), which crystallized late in CE-5 basalts (D. Zhang et al., 2022; Boschi et al., 2023). These low-Mg# samples have similar δ^{56}Fe and variable δ^{26}Mg. An olivine sample (F123) and two ilmenite samples (F115 and F117) show large positive δ^{26}Mg fractionation relative to the bulk CE-5 basalts (Figure 1).

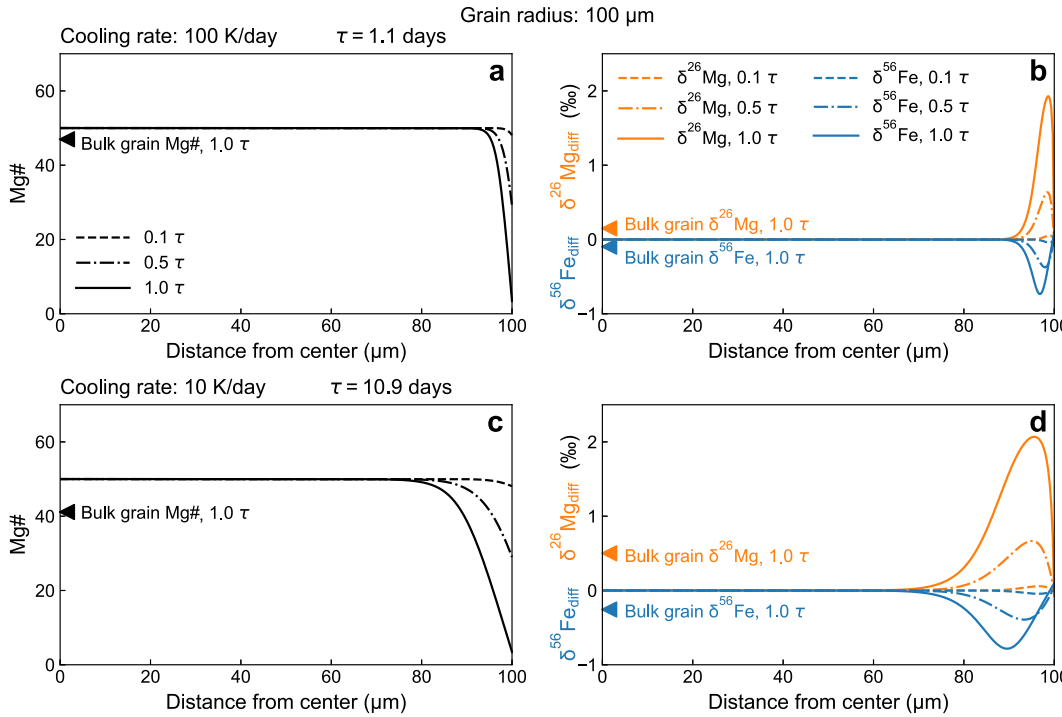

Figure 2. Evolution of isotopic compositions and Mg# in olivine grains during diffusion modeled using different cooling rates and a fixed grain radius. Cooling rates of 100 K/day (a and b) and 10 K/day (c and d) are used, which correspond to cooling timescales (τ) of 1.1 and 10.9 days, respectively. An initial Mg# of 50 and a grain radius of 100 μm are used. The modeled Mg# (a and c), $\delta^{56}Fe_{diff}$, and $\delta^{26}Mg_{diff}$ (b and d) profiles at 0.1, 0.5, and 1 τ are shown as curves, where $\delta^{56}Fe_{diff}$ and $\delta^{26}Mg_{diff}$ are relative to the initial isotopic composition. The triangles represent the modeled final chemical and isotopic compositions of bulk grains.

Due to the high Fe content, Fe–Mg inter-diffusion in low-Mg# grains would cause limited Fe isotope fractionation and substantial positive Mg isotope fractionation, consistent with the measured data of these samples. Because the olivine samples have recorded different diffusion processes in both high-Mg# and low-Mg# olivines, we focus on modeling the Fe–Mg inter-diffusion in olivine grains.

Different diffusion scenarios were modeled using various sets of parameters. The diffusion coefficient, the key parameter controlling the speed of diffusion, is dependent on temperature (Dohmen & Chakraborty, 2007). Ganguly and Tirone (1999) developed generalized formulation of diffusion closure to arbitrary extents of diffusion, demonstrating that the extent of diffusive resetting depends on cooling rate, grain size, and initial temperature, such that: (a) higher cooling rates suppress diffusive resetting by reducing the duration of diffusion; (b) larger grains facilitate preservation of original core composition established at the initial temperature; (c) higher initial temperature enhances the diffusion coefficient at the onset of cooling, promoting more extensive modification of the mineral interior.

The Fe–Mg inter-diffusion in olivine grains is driven by the compositional contrast between the evolving melt and the olivine grains (Dauphas et al., 2010; Teng et al., 2011). In our diffusion modeling, the temperature interval over which diffusion occurs is fixed for each mineral grain: diffusion begins at the crystallization temperature of the grain and terminates at 1024°C, the temperature at which crystallization of the bulk rock is completed and the melt phase is effectively exhausted in the MELTS model. Temperature is assumed to vary linearly with time (Dauphas et al., 2010). Consequently, the cooling rate controls the duration of diffusion and thus determines the resultant diffusion profiles within mineral grains (Figure 2). High cooling rates, such as 100 K/day over 1.1 days, restrict diffusion to narrow rims and produce minimal bulk-grain isotopic fractionation. Lower cooling rates, such as 10 K/day over 10.9 days, permit diffusion over greater distances and cause substantial fractionation. The magnitude of bulk-grain isotopic fractionation also varies with grain size for a given cooling rate (Figure S2 in Supporting Information S1). Systematic comparison between modeled results and measured isotopic

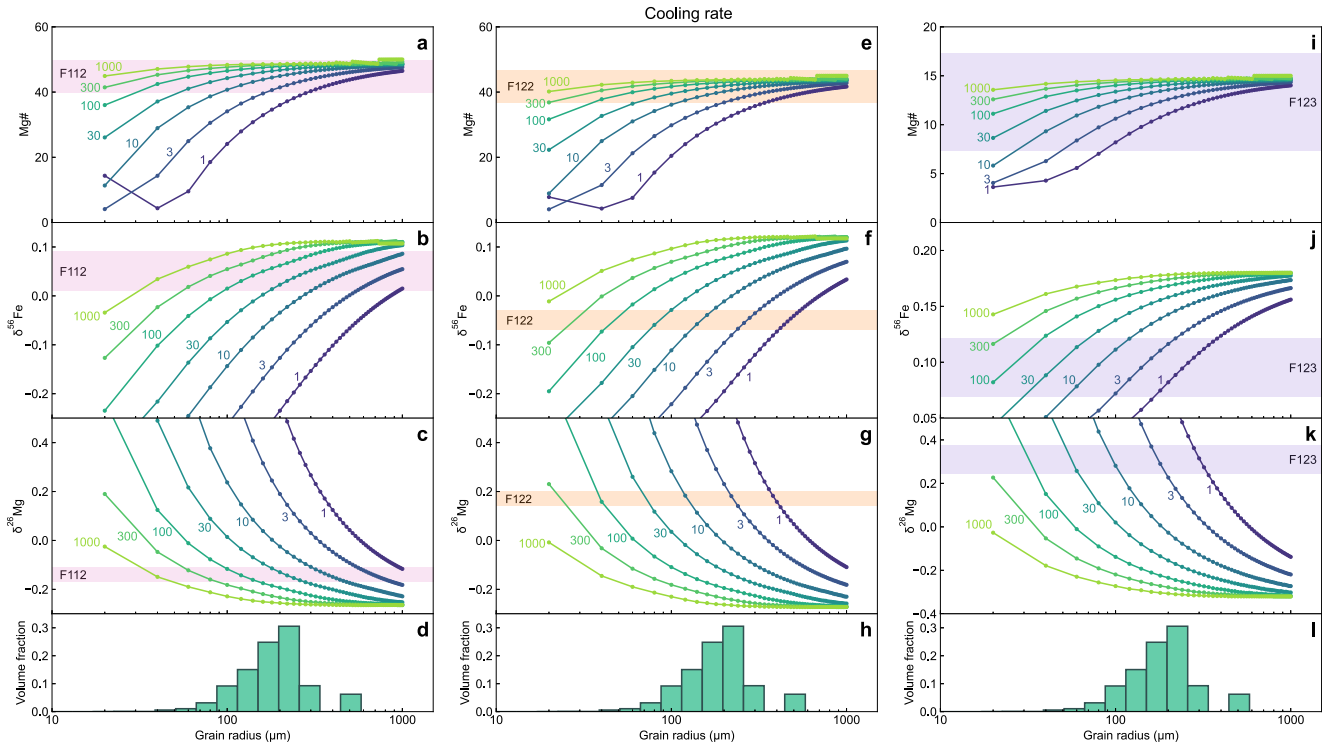

Figure 3. Evaluation of the cooling rates of F112, F122, and F123. The modeled Mg# and isotopic compositions are shown as a function of grain radius and cooling rate. Modeled results with different cooling rates (colored numbers, in °C/day) and grain radii are compared with the measured Mg# (a, e, and i), δ^{56}Fe (b, f, and j), and δ^{26}Mg (c, g, and k). The initial Mg# is fixed at 50 in the modeling. The measured distribution of olivine grain sizes is presented as volume fractions of the clast (the same results are shown in d, h, and l for comparison with other panels).

compositions, combined with the observed size distribution of olivine grains, provides constraints on the cooling history of the basalt clast.

4.2. Cooling History Inferred by Diffusion Modeling

The final δ^{56}Fe, δ^{26}Mg, and Mg# of bulk olivine grains were modeled using different initial Mg#, cooling rates, and grain radii. Our modeling results show that the slope of δ^{56}Fe–δ^{26}Mg correlation curve is dependent on the initial Mg# of the olivine grain (Figure S3 in Supporting Information S1), consistent with literature results (Dauphas et al., 2010; Teng et al., 2011). The curves in Mg#–δ^{56}Fe and Mg#–δ^{26}Mg plots are also dependent on the initial Mg# (Figure S3 in Supporting Information S1). The modeled bulk-grain δ^{56}Fe, δ^{26}Mg, and Mg# vary with different cooling rates and grain sizes, but the curves fall on the same trajectory (Figure S4 in Supporting Information S1). Therefore, the initial Mg# of olivines can be directly constrained using these curves (Figure S3 in Supporting Information S1).

For olivine samples with substantial isotope fractionation, all the three plots show consistent initial Mg# values. Based on the modeling results in Figure S3 in Supporting Information S1, the two olivine samples with high Mg# also have high initial Mg# values (~50 for F112 and ~45 for F122). Such an initial Mg# of 50 is similar to those at the cores of CE-5 olivines and clinopyroxenes (Y. Li et al., 2025; Luo et al., 2023; Tian et al., 2021, 2023). The olivine sample that shows large positive δ^{26}Mg fractionation (F123) falls on the curves corresponding to a low initial Mg# of ~15. The other olivine samples, which have Mg# lower than 10, do not fall on the curves (Figure S3 in Supporting Information S1), suggesting late crystallization and limited diffusion. Using the inferred initial Mg#, the crystallization temperatures can be estimated based on the magmatic evolution modeling results, which are ~1133°C, ~1113°C, and ~1053°C for F112, F122, and F123, respectively.

Using the inferred initial Mg# and crystallization temperature, the cooling rate of each sample can be constrained. Combined with the radii of olivine grains that make up the majority of the volume of olivine (100–300 μm, Figure 3d), the modeling results can be compared with the measured data. Our results show that Mg# is insensitive

to the cooling rate (Figures 3a, 3e, and 3i). On the contrary, isotopic compositions are sensitive to cooling rate and grain size. For F112, the δ^{56}Fe and δ^{26}Mg results modeled with cooling rates of 30–100°C/day and grain radii of 100–300 μm are consistent with the measured data (Figures 3b and 3c). For F122, the measured isotopic data imply a lower cooling rate of 3–10°C/day (Figures 3f and 3g). For F123, the measured large δ^{26}Mg fractionation is consistent with cooling rates of 1–10°C/day (Figures 3j and 3k). These results suggest that the difference between the isotopic compositions of F112 and F122 likely resulted from a decrease in the cooling rate, and F123 experienced even slower cooling than F122. Although F112 and F122 have similar Mg# values, the difference in their modeled cooling rates is greater than that between F122 and F123. This apparent discrepancy is not a modeling artifact but results from the distinct isotopic compositions of F112 and F122, reflecting either a pronounced early-stage decrease in cooling rate or uncertainties arising from grain size constraints. A detailed discussion of this apparent discrepancy is presented in Supporting Information S1.

In addition to the modeled isotopic compositions of bulk olivines, the modeled isotopic profiles can be compared with published in situ isotopic data. Higher cooling rates tend to cause isotopic fractionation at grain rims, while low cooling rates facilitate equilibrium and lead to isotopic fractionation at grain cores (Figure 2). The recently reported in situ Fe isotopic data of basalt clasts and olivine fragments from CE-5 lunar soil samples show that olivines with radii of ∼100 μm are more enriched in light Fe isotopes at rims than their cores (Y. Li et al., 2025). For an olivine with 100 μm radius and initial Mg# of 52 (core composition of an olivine grain; Y. Li et al., 2025), modeled isotopic profiles at cooling rates ≥1°C/day yield lower δ^{56}Fe at the rims (Figure S6 in Supporting Information S1), indicating cooling at rates of at least 1°C/day.

4.3. Implications for the Evolution of CE-5 Basalts

Previous studies have observed various textures of CE-5 basalts, implying different cooling rates in different parts of the lava flow (Boschi et al., 2023; Luo et al., 2023; Tian et al., 2021, 2023). The crystal size distributions of CE-5 basalts suggest residence time from several to hundreds of days (Luo et al., 2023; Tian et al., 2023). The cooling rates were estimated based on crystal size distribution, plagioclase width, and liquid immiscibility microstructure, spanning from <7.2°C/day during late-stage crystallization (Jin et al., 2024) to as high as ∼4000°C/day in a rapidly cooled clast (Z. Wang, Tian, et al., 2023), with intermediate values (∼40–2000°C/day) also reported (Jiang et al., 2022; Neal et al., 2022; Webb et al., 2022).

In addition, Mg# zoning patterns in olivines and clinopyroxenes are suggested to be the result of Fe–Mg inter-diffusion that reflect different cooling histories of CE-5 basalts (Luo et al., 2023; Tian et al., 2023; Z. Wang, Wang, et al., 2023). The Mg# zonation, however, can either result from crystal growth in an evolving melt or Fe–Mg inter-diffusion (Dauphas et al., 2010; Teng et al., 2011). The effects of crystal growth on chemical zonation need to be excluded by focusing on internal zoning (Luo et al., 2023) or monitoring the contribution of crystal growth using other elements (Tian et al., 2023; Z. Wang, Wang, et al., 2023). On the contrary, the anti-correlated Fe and Mg isotope fractionation can be unambiguously ascribed to the chemical diffusion process (Dauphas et al., 2010; Teng et al., 2011).

Our isotope measurements and modeling suggest that the cooling rate decreased from 30–100°C/day for the earliest-forming olivines to 1–10°C/day for the other olivines (and likely other late-forming minerals). In previous studies of the CE-5 basalts, the cooling rate has been presented as a single value for each basalt clast, representing the entire cooling history of that clast. Our results of different mineral grains from the same clast, which crystallized sequentially, show a decrease in cooling rate with decreasing Mg# values (Figure 4a). This change in cooling rate provides insights into the temporal evolution of thermal conditions for the studied CE-5 basalt clast. We propose two potential scenarios to interpret the decrease in cooling rate.

In Scenario 1, we consider the change in thermal conditions during and after eruption. The drop in cooling rate by roughly an order of magnitude is similar to the cooling path of olivine phenocrysts from the Kilauea Iki lava lake, which cooled rapidly during eruption and cooled more slowly in the lava lake (Helz et al., 2014; Sio et al., 2013). Therefore, the earliest-forming olivine (F112) potentially crystallized before or during eruption, cooling rapidly in the eruption period, and the other minerals crystallized after eruption and cooled slowly in the lava flow (Scenario 1; Figure 4b). Combining this cooling path with the estimated crystallization temperatures of olivine samples, our results potentially constrain the eruption temperature of CE-5 basalts to ∼1113–1133°C. This temperature is consistent with the lower limit of magma storage temperature (1150 ± 50°C) of CE-5 basalts (Luo et al., 2023).

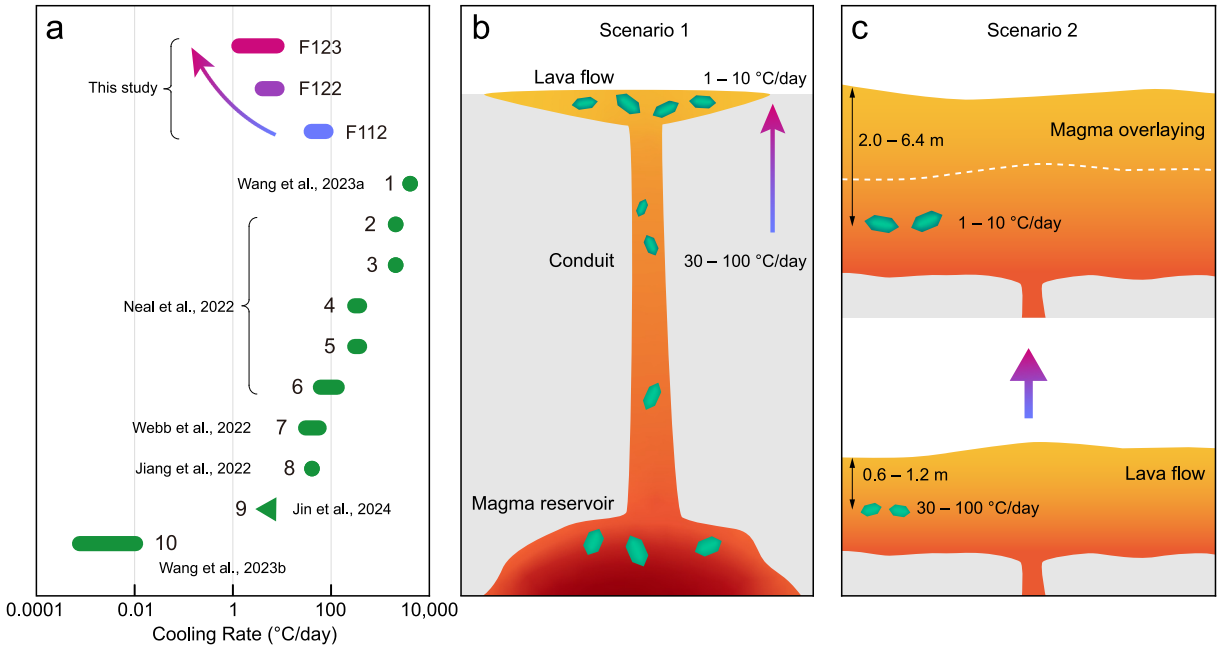

Figure 4. Temporal evolution of cooling rate and thermal condition. (a) Decreasing cooling rate of the olivine samples in the studied clast, compared with previously reported cooling rates of CE-5 basalts. The bars represent the reported ranges of cooling rates. The triangle represents the upper limit of cooling rate. The numbered labels correspond to the following samples of CE-5 basalts and the data sources: 1: CE5C0800YJYX005GP (Z. Wang, Tian, et al., 2023); 2: B015-04; 3: B016-04; 4: B015-02; 5: B015-03; 6: 329 (Neal et al., 2022); 7: B1 (Webb et al., 2022); 8: CE5C0000YJYX065 (Jiang et al., 2022); 9: basalt clast in CE5C0400YJFM (Jin et al., 2024); 10: CE5C0800YJYX013GP (Z. Wang, Wang, et al., 2023). (b) Scenario 1: rapid cooling during eruption in the conduit and slow cooling in the lava flow. (c) Scenario 2: decrease in cooling rate due to magma overlaying. The arrows represent the decrease in the cooling rate from 30–100°C/day to 1–10°C/day.

Alternatively, if the clast was overlayed by later erupted magma, the cooling rate might decrease (Scenario 2; Figure 4c). Using the relation between cooling rate and buried depth calibrated by cooling experiments of Apollo mare basalts (Walker et al., 1976), the buried depth can be calculated as 0.6–1.2 m for 30–100°C/day and 2.0–6.4 m for 1–10°C/day. Previous studies suggested episodic eruptions at the Chang'e-5 landing site, producing multiple layers of mare basalts, which have total thicknesses ranging from tens to hundreds of meters (J. Du et al., 2022; Tian et al., 2023; Z. Wang, Wang, et al., 2023). Therefore, the studied clast remained in a shallow region of the lava flow. Our results potentially indicate a substantial change in cooling rate (approximately an order of magnitude) resulting from a relatively small increase in burial depth (up to 5.8 m).

As our isotopic results directly reflect the consequences of Fe–Mg inter-diffusion, discerning whether the change in cooling rate resulted from different thermal conditions from conduit to lava flow (Scenario 1) or magma overlaying (Scenario 2) is difficult. Nonetheless, a temporal change in thermal conditions in the cooling history of the CE-5 basalt clast can be confirmed. Future studies that combine minerology and cooling rate estimation of different minerals in the same clast may provide more insights into the detailed thermal history of CE-5 basalts.

5. Conclusions

Minerals separated from a mm-sized CE-5 basalt clast show ~0.3‰ and ~0.8‰ variations for δ^{56}Fe and δ^{26}Mg, respectively. The negative correlation between δ^{56}Fe and δ^{26}Mg suggest that Fe–Mg inter-diffusion caused the isotope fractionation. We systematically modeled the diffusion-driven fractionation with different initial compositions, cooling rates, and grain sizes and compared them with the measured data. This approach can be used as a thermometer to trace the cooling history of igneous rocks.

Our results place new constraints on the evolution path for the crystallization and cooling of CE-5 basalts. In a highly evolved lunar basaltic melt, the olivines with Mg# of ~50 crystallized before or during eruption. The melt erupted at approximately 1113–1133°C and cooled rapidly on 30–100°C/day during the eruption period. After eruption, minerals with lower Mg contents crystallized, including fayalite, plagioclase, ilmenite, and Fe-rich pigeonites. These minerals cooled slowly at 1–10°C/day in the lava flow. In addition, magma overlaying

might have increased the buried depth of the clast, contributing to the cooling rate decrease. Our results demonstrate that Fe–Mg inter-diffusion is the major cause of mineral-scale Fe and Mg isotope fractionation in CE-5 basalts, which have recorded the temporal evolution of the thermal conditions in the crystallization and cooling histories.

Conflict of Interest

The authors declare no conflicts of interest relevant to this study.

Availability Statement

The chemical and isotopic data are presented in Supporting Information S1. The diffusion modeling code and all data in this study have been uploaded to a Zenodo repository (Shuai, 2025). We used the MELTS software (https://melts.ofm-research.org/) and ImageJ (https://imagej.net/ij/) with the BoneJ plugin (https://github.com/bonej-org/BoneJ2).

Acknowledgments
This paper benefited from constructive comments from two anonymous reviewers and editor Jean-Pierre Williams. The authors thank Zhiguang Xia and Xiang-Long Luo for their help with the isotopic measurements. This work was supported by the National Natural Science Foundation of China (NSFC; No. 42425301 to WL and No. 42508025 to KS), the China Postdoctoral Science Foundation (CPSF; No. 2025M773192), the Postdoctoral Fellowship Program of CPSF (No. GZC20252094), and Jiangsu Funding Program for Excellent Postdoctoral Talent (No. 2025ZB246) to KS. We are grateful to the China National Space Administration for providing the Chang'E-5 basalt clast.

References

An, S., Chen, J., Boschi, S., & Li, W. (2023). Significantly enhanced robustness of K isotope analysis by collision cell MC-ICP-MS and its application to the returned lunar samples by China's Chang'e-5 project. *Analytical Chemistry*, *95*(4), 2140–2145. https://doi.org/10.1021/acs.analchem.2c03989

Asimow, P. D., & Ghiorso, M. S. (1998). Algorithmic modifications extending MELTS to calculate subsolidus phase relations. *American Mineralogist*, *83*(9–10), 1127–1132. https://doi.org/10.2138/am-1998-9-1022

Boschi, S., Wang, X., Hui, H., Yin, Z., Guan, Y., Hu, H., et al. (2023). Compositional variability of 2.0-Ga lunar basalts at the Chang'e-5 landing site. *Journal of Geophysical Research: Planets*, *128*(5), e2022JE007627. https://doi.org/10.1029/2022JE007627

Brzozowski, M. J., Good, D. J., Yan, W., Wu, C., An, S., & Li, W. (2022). Mg–Fe isotopes link the geochemical complexity of the coldwell complex, midcontinent rift to metasomatic processes in the mantle. *Journal of Petrology*, *63*(8), egac081. https://doi.org/10.1093/petrology/egac081

Che, X., Nemchin, A., Liu, D., Long, T., Wang, C., Norman Marc, D., et al. (2021). Age and composition of young basalts on the Moon, measured from samples returned by Chang'e-5. *Science*, *374*(6569), 887–890. https://doi.org/10.1126/science.abl7957

Dauphas, N., Roskosz, M., Alp, E. E., Neuville, D. R., Hu, M. Y., Sio, C. K., et al. (2014). Magma redox and structural controls on iron isotope variations in Earth's mantle and crust. *Earth and Planetary Science Letters*, *398*, 127–140. https://doi.org/10.1016/j.epsl.2014.04.033

Dauphas, N., Teng, F.-Z., & Arndt, N. T. (2010). Magnesium and iron isotopes in 2.7 Ga Alexo komatiites: Mantle signatures, no evidence for Soret diffusion, and identification of diffusive transport in zoned olivine. *Geochimica et Cosmochimica Acta*, *74*(11), 3274–3291. https://doi.org/10.1016/j.gca.2010.02.031

Dohmen, R., & Chakraborty, S. (2007). Erratum to "Fe–Mg diffusion in olivine II: Point defect chemistry, change of diffusion mechanisms and a model calculation of diffusion coefficients in natural olivine.". *Physics and Chemistry of Minerals*, *34*(8), 597–598. https://doi.org/10.1007/s00269-007-0185-3

Doube, M. (2021). Multithreaded two-pass connected components labelling and particle analysis in ImageJ. *Royal Society Open Science*, *8*(3), 201784. https://doi.org/10.1098/rsos.201784

Du, D.-H., Luo, X.-L., Wang, X.-L., Palmer, M. R., Ersoy, E. Y., & Li, W. (2024). A recipe for making potassium-rich magmas in collisional orogens: New insights from K and Fe isotopes. *Earth and Planetary Science Letters*, *632*, 118642. https://doi.org/10.1016/j.epsl.2024.118642

Du, J., Fa, W., Gong, S., Liu, Y., Qiao, L., Tai, Y., et al. (2022). Thicknesses of mare basalts in the Chang'E-5 landing region: Implications for the late-stage volcanism on the Moon. *Journal of Geophysical Research: Planets*, *127*(8), e2022JE007314. https://doi.org/10.1029/2022JE007314

Ganguly, J., & Tirone, M. (1999). Diffusion closure temperature and age of a mineral with arbitrary extent of diffusion: Theoretical formulation and applications. *Earth and Planetary Science Letters*, *170*(1–2), 131–140. https://doi.org/10.1016/S0012-821X(99)00089-8

Ghiorso, M. S., & Sack, R. O. (1995). Chemical mass transfer in magmatic processes IV. A revised and internally consistent thermodynamic model for the interpolation and extrapolation of liquid-solid equilibria in magmatic systems at elevated temperatures and pressures. *Contributions to Mineralogy and Petrology*, *119*(2–3), 197–212. https://doi.org/10.1007/BF00307281

He, Y., Ke, S., Teng, F.-Z., Wang, T., Wu, H., Lu, Y., & Li, S. (2015). High-precision iron isotope analysis of geological reference materials by high-resolution MC-ICP-MS. *Geostandards and Geoanalytical Research*, *39*(3), 341–356. https://doi.org/10.1111/j.1751-908X.2014.00304.x

Helz, R. T., Clague, D. A., Sisson, T. W., & Thornber, C. R. (2014). Petrologic insights into basaltic volcanism at historically active Hawaiian volcanoes. In *Characteristics of Hawaiian volcanoes* (Vol. 1801, pp. 237–292). US Geological Survey Professional Paper 1801.

Huang, F., Chakraborty, P., Lundstrom, C. C., Holmden, C., Glessner, J. J. G., Kieffer, S. W., & Lesher, C. E. (2010). Isotope fractionation in silicate melts by thermal diffusion. *Nature*, *464*(7287), 396–400. https://doi.org/10.1038/nature08840

Jiang, Y., Kang, J., Liao, S., Elardo, S. M., Zong, K., Wang, S., et al. (2023). Fe and Mg isotope compositions indicate a hybrid mantle source for young Chang'e 5 mare basalts. *The Astrophysical Journal Letters*, *945*(2), L26. https://doi.org/10.3847/2041-8213/acbd31

Jiang, Y., Li, Y., Liao, S., Yin, Z., & Hsu, W. (2022). Mineral chemistry and 3D tomography of a Chang'E 5 high-Ti basalt: Implication for the lunar thermal evolution history. *Science Bulletin*, *67*(7), 755–761. https://doi.org/10.1016/j.scib.2021.12.006

Jin, Z., Hou, T., Zhu, M.-H., Zhang, Y., & Namur, O. (2024). Late-stage microstructures in Chang'E-5 basalt and implications for the evolution of lunar ferrobasalt. *American Mineralogist*, *110*(4), 560–569. https://doi.org/10.2138/am-2024-9448

Li, C., Hu, H., Yang, M.-F., Pei, Z.-Y., Zhou, Q., Ren, X., et al. (2022). Characteristics of the lunar samples returned by the Chang'E-5 mission. *National Science Review*, *9*(2), nwab188. https://doi.org/10.1093/nsr/nwab188

Li, Q.-L., Zhou, Q., Liu, Y., Xiao, Z., Lin, Y., Li, J. H., et al. (2021). Two billion-year-old volcanism on the Moon from Chang'E-5 basalts. *Nature*, *600*(7887), 54–58. https://doi.org/10.1038/s41586-021-04100-2

Li, Y., Wang, Z., Qian, Y., Zhang, W., Feng, Y., Liu, H., et al. (2025). Iron isotopes of Chang'e-5 soil and mineral components: Implications for post-eruption processes on lunar surface. *Icarus*, *426*, 116362. https://doi.org/10.1016/j.icarus.2024.116362

Liu, Y., Spicuzza, M. J., Craddock, P. R., Day, J. M. D., Valley, J. W., Dauphas, N., & Taylor, L. A. (2010). Oxygen and iron isotope constraints on near-surface fractionation effects and the composition of lunar mare basalt source regions. *Geochimica et Cosmochimica Acta*, *74*(21), 6249–6262. https://doi.org/10.1016/j.gca.2010.08.008

Luo, B., Wang, Z., Song, J., Qian, Y., He, Q., Li, Y., et al. (2023). The magmatic architecture and evolution of the Chang'e-5 lunar basalts. *Nature Geoscience*, *16*(4), 301–308. https://doi.org/10.1038/s41561-023-01146-x

Neal, C. R., Valenciano, J. L., Che, X., Shi, Y., Liu, D., Tao, L., et al. (2022). Crystal size distribution of ilmenite in Chang'e 5 basalt clasts. In *53rd lunar and planetary science conference* (p. 2353).

Oeser, M., Dohmen, R., Horn, I., Schuth, S., & Weyer, S. (2015). Processes and time scales of magmatic evolution as revealed by Fe–Mg chemical and isotopic zoning in natural olivines. *Geochimica et Cosmochimica Acta*, *154*, 130–150. https://doi.org/10.1016/j.gca.2015.01.025

Oeser, M., Dohmen, R., & Weyer, S. (2026). Fe-Mg in olivine: Simultaneous experimental determination of the diffusion-driven isotope fractionation along with tracer- and inter-diffusion coefficients. *Geochimica et Cosmochimica Acta*, *413*, 48–66. https://doi.org/10.1016/j.gca.2025.09.036

Okabayashi, S., Yokoyama, T., Hirata, T., Terakado, K., & Galimov, E. M. (2019). Iron isotopic composition of very low-titanium basalt deduced from the iron isotopic signature in Luna 16, 20, and 24 soils. *Geochimica et Cosmochimica Acta*, *269*, 1–14. https://doi.org/10.1016/j.gca.2019.10.020

Poitrasson, F., Zambardi, T., Magna, T., & Neal, C. R. (2019). A reassessment of the iron isotope composition of the Moon and its implications for the accretion and differentiation of terrestrial planets. *Geochimica et Cosmochimica Acta*, *267*, 257–274. https://doi.org/10.1016/j.gca.2019.09.035

Qian, Y., She, Z., He, Q., Xiao, L., Wang, Z., Head, J. W., et al. (2023). Mineralogy and chronology of the young mare volcanism in the Procellarum-KREEP-Terrane. *Nature Astronomy*, *7*(3), 287–297. https://doi.org/10.1038/s41550-022-01862-1

Richter, F. M., Watson, E. B., Mendybaev, R., Dauphas, N., Georg, B., Watkins, J., & Valley, J. (2009). Isotopic fractionation of the major elements of molten basalt by chemical and thermal diffusion. *Geochimica et Cosmochimica Acta*, *73*(14), 4250–4263. https://doi.org/10.1016/j.gca.2009.04.011

Sedaghatpour, F., & Jacobsen, S. B. (2019). Magnesium stable isotopes support the lunar magma ocean cumulate remelting model for mare basalts. *Proceedings of the National Academy of Sciences of the United States of America*, *116*(1), 73–78. https://doi.org/10.1073/pnas.1811377115

Sedaghatpour, F., Teng, F.-Z., Liu, Y., Sears, D. W. G., & Taylor, L. A. (2013). Magnesium isotopic composition of the Moon. *Geochimica et Cosmochimica Acta*, *120*, 1–16. https://doi.org/10.1016/j.gca.2013.06.026

Shahar, A., Young, E. D., & Manning, C. E. (2008). Equilibrium high-temperature Fe isotope fractionation between fayalite and magnetite: An experimental calibration. *Earth and Planetary Science Letters*, *268*(3–4), 330–338. https://doi.org/10.1016/j.epsl.2008.01.026

Shearer, C. K. (2006). Thermal and magmatic evolution of the Moon. *Reviews in Mineralogy and Geochemistry*, *60*(1), 365–518. https://doi.org/10.2138/rmg.2006.60.4

Shuai, K. (2025). Numerical model of diffusion-driven Fe-Mg isotopic fractionation [Dataset]. *Zenodo*. https://doi.org/10.5281/zenodo.19591852

Sio, C. K. I., & Dauphas, N. (2017). Thermal and crystallization histories of magmatic bodies by Monte Carlo inversion of Mg-Fe isotopic profiles in olivine. *Geology*, *45*(1), 67–70. https://doi.org/10.1130/G38056.1

Sio, C. K. I., Dauphas, N., Teng, F.-Z., Chaussidon, M., Helz, R. T., & Roskosz, M. (2013). Discerning crystal growth from diffusion profiles in zoned olivine by in situ Mg–Fe isotopic analyses. *Geochimica et Cosmochimica Acta*, *123*, 302–321. https://doi.org/10.1016/j.gca.2013.06.008

Sio, C. K. I., Roskosz, M., Dauphas, N., Bennett, N. R., Mock, T., & Shahar, A. (2018). The isotope effect for Mg-Fe interdiffusion in olivine and its dependence on crystal orientation, composition and temperature. *Geochimica et Cosmochimica Acta*, *239*, 463–480. https://doi.org/10.1016/j.gca.2018.06.024

Sossi, P. A., & Moynier, F. (2017). Chemical and isotopic kinship of iron in the Earth and Moon deduced from the lunar Mg-Suite. *Earth and Planetary Science Letters*, *471*, 125–135. https://doi.org/10.1016/j.epsl.2017.04.029

Teng, F.-Z., Dauphas, N., Helz, R. T., Gao, S., & Huang, S. (2011). Diffusion-driven magnesium and iron isotope fractionation in Hawaiian olivine. *Earth and Planetary Science Letters*, *308*(3–4), 317–324. https://doi.org/10.1016/j.epsl.2011.06.003

Teng, F.-Z., Li, W.-Y., Ke, S., Yang, W., Liu, S.-A., Sedaghatpour, F., et al. (2015). Magnesium isotopic compositions of international geological reference materials. *Geostandards and Geoanalytical Research*, *39*(3), 329–339. https://doi.org/10.1111/j.1751-908X.2014.00326.x

Teng, F.-Z., Wadhwa, M., & Helz, R. T. (2007). Investigation of magnesium isotope fractionation during basalt differentiation: Implications for a chondritic composition of the terrestrial mantle. *Earth and Planetary Science Letters*, *261*(1–2), 84–92. https://doi.org/10.1016/j.epsl.2007.06.004

Tian, H.-C., Wang, H., Chen, Y., Yang, W., Zhou, Q., Zhang, C., et al. (2021). Non-KREEP origin for Chang'e-5 basalts in the Procellarum KREEP Terrane. *Nature*, *600*(7887), 59–63. https://doi.org/10.1038/s41586-021-04119-5

Tian, H.-C., Zhang, C., Teng, F.-Z., Long, Y.-J., Li, S.-G., He, Y., et al. (2020). Diffusion-driven extreme Mg and Fe isotope fractionation in Panzhihua ilmenite: Implications for the origin of mafic intrusion. *Geochimica et Cosmochimica Acta*, *278*, 361–375. https://doi.org/10.1016/j.gca.2019.10.004

Tian, H.-C., Zhang, C., Yang, W., Du, J., Chen, Y., Xiao, Z., et al. (2023). Surges in volcanic activity on the Moon about two billion years ago. *Nature Communications*, *14*(1), 3734. https://doi.org/10.1038/s41467-023-39418-0

Walker, D., Longhi, J., Kirkpatrick, R. J., & Hays, J. F. (1976). Differentiation of an Apollo 12 picrite magma. In *7th lunar and planetary science conference* (pp. 1365–1389).

Wang, K., Jacobsen, S. B., Sedaghatpour, F., Chen, H., & Korotev, R. L. (2015). The earliest Lunar Magma Ocean differentiation recorded in Fe isotopes. *Earth and Planetary Science Letters*, *430*, 202–208. https://doi.org/10.1016/j.epsl.2015.08.019

Wang, W., Wu, Z., Huang, S., & Huang, F. (2023). First-principles investigation of equilibrium magnesium isotope fractionation among mantle minerals: Review and new data. *Earth-Science Reviews*, *237*, 104315. https://doi.org/10.1016/j.earscirev.2023.104315

Wang, Z., Tian, W., Ma, B., Liu, P.-P., Pei, J., Chen, Z., et al. (2023). Crystallization kinetics of a fastest-cooling young mare basalt of Chang'E-5. *Science Bulletin*, *68*(15), 1621–1624. https://doi.org/10.1016/j.scib.2023.06.036

Wang, Z., Wang, W.-(R. Z.), Tian, W., Li, H., Qian, Y., Pei, J., et al. (2023). Cooling rate of clinopyroxene reveals the thickness and effusion volume of Chang'E-5 basaltic flow units. *Icarus*, *394*, 115406. https://doi.org/10.1016/j.icarus.2022.115406

Webb, S., Neal, C. R., Che, X., Shi, Y., Liu, D., Tao, L., et al. (2022). Crystal size distribution of plagioclase in basalt fragments from Oceanus Procellarum recovered by Chang'e-5. In *53rd lunar and planetary science conference* (p. 2896).

Weyer, S., Anbar, A. D., Brey, G. P., Münker, C., Mezger, K., & Woodland, A. B. (2005). Iron isotope fractionation during planetary differentiation. *Earth and Planetary Science Letters*, *240*(2), 251–264. https://doi.org/10.1016/j.epsl.2005.09.023

Wiesli, R. A., Beard, B. L., Taylor, L. A., & Johnson, C. M. (2003). Space weathering processes on airless bodies: Fe isotope fractionation in the lunar regolith. *Earth and Planetary Science Letters*, *216*(4), 457–465. https://doi.org/10.1016/S0012-821X(03)00552-1

Xiong, Z., Huang, S., & Van Orman, J. A. (2023). Empirical constraints on the mass dependence of isotope diffusion in minerals by modeling sub-solidus exchange: Calcium isotopes in the two-pyroxene system. *Geochimica et Cosmochimica Acta*, *341*, 105–115. https://doi.org/10.1016/j.gca.2022.11.022

Zhang, D., Su, B., Chen, Y., Yang, W., Mao, Q., & Jia, L.-H. (2022). Titanium in olivine reveals low-Ti origin of the Chang'E-5 lunar basalts. *Lithos*, *414–415*, 106639. https://doi.org/10.1016/j.lithos.2022.106639

Zhang, H., Yang, W., Zhang, D., Tian, H., Ruan, R., Hu, S., et al. (2024). Long-term reduced lunar mantle revealed by Chang'e-5 basalt. *Nature Communications*, *15*(1), 8328. https://doi.org/10.1038/s41467-024-52710-x